Evaluation of the Mono-static Microwave Radar Algorithms for Breast Imaging

Evgeny Kirshin*, Guangran K. Zhu*, Milica Popovich*, Mark Coates*
*Department of Electrical and Computer Engineering
McGill University, Montréal, Canada
{evgeny.kirshin, guangran.zhu, milica.popovich, mark.coates}@mcgill.ca

***Abstract*—Microwave radar imaging for breast cancer detection is one promising technique to replace/supplement X-ray mammography and MRI. Previously developed imaging algorithms have been applied to the signals generated from breast models comprising large dielectric contrast and relatively homogeneous tissue. This study investigates five imaging algorithms applied to the signals generated from more realistic models. The signals were generated from the finite-difference time-domain simulations of the microwave interaction with breast models. We find that, under a good estimate of the average dielectric properties of the tissue and tumor, the generalized likelihood ratio test algorithm is capable of detecting tumors, in the sense of a good signal-to-interference-and-noise ratio in the presence of reduced dielectric contrast and increased tissue heterogeneity. This establishes the motivation to estimate the average tissue properties and extend the algorithm to handle multi-static signals for microwave breast imaging.**

I. Introduction and Background

Microwave radar imaging was proposed in the late 1990s as a screening method to complement the conventional X-ray mammography for breast cancer detection. The underlying physical principle that enables tumour detection is the contrast in the dielectric properties between healthy and tumorous tissue. Recent characterization of the dielectric properties of the breast tissue suggests that high contrast may be observed only between the adipose-dominant and tumorous tissue [1], [2]. The contrast between the glandular-dominant and tumorous tissue often does not exceed 1.1. This fact complicates the breast imaging tasks for tumour detection, especially in cases where the tumour is located inside the glandular tissue.

Microwave imaging algorithms have been studied previously and have been applied to the signals generated from two-dimensional (2-D) or simple three-dimensional (3-D) breast models with large dielectric contrast and relatively homogeneous tissues. Mostly known algorithms presented in the literature include the delay-and-sum (DAS) algorithm [3], [4], the delay-multiply-and-sum (DMAS) algorithm [5], the mono-static space-time beamformer (STB) algorithms [6], [7], the time-reversal algorithm [8], the generalized likelihood ratio test (GLRT) algorithm [9] as well as the mono-static robust capon beamformer (RCB) algorithm [10] and the multi-static adaptive microwave imaging (MAMI) algorithm [11], which is a two-stage implementation of the RCB algorithm.

Currently, the STB algorithm has been extended to handle multi-static signals [12], and the MAMI algorithm has been modified [13] to exploit the one-to-many relation between the transmit and receive antennas in the signals, which was previously neglected. They have shown improved performance, when being applied to the signals generated from more realistic breast models based on [1], [2].

In this paper, we report on the study of applying five imaging algorithms to the signals from 2-D breast models. They include DAS, DMAS, STB, GLRT and RCB algorithms. We find that the DAS and DMAS algorithms exhibit small localization error in the generated images, but they fail in the scenarios of high breast tissue density. The STB algorithm has an improved capability to image breasts due to its rejection of interference, but is prone to localization errors. Under a good estimate of the average dielectric properties of the tissue and tumor, the generalized likelihood ratio test algorithm is capable of detecting tumors, in the sense of a good signal-to-interference-and-noise ratio. Since the microwave breast imaging strives to achieve the best signal-to-interference-and-noise ratio, the GLRT algorithm holds the promise for this aim. As the current GLRT algorithm handles mono-static signals, this study motivates to extend the GLRT algorithm to handle multi-static signals.

This paper is structured as follows. Section II presents the five imaging algorithms and Section III presents the design of numerical simulations. Section IV discusses the imaging results based on the common performance metrics. This is followed by Section V to conclude the paper and delineate our future work.

II. Imaging Algorithms

Microwave radar imaging algorithms exploit the space and time-invariance of the wave equation. They synthetically align the received signals in time, and attempt to draw the scattering properties at the synthetic focal point. This avoids solving the ill-posed and computationally-demanding inverse problem as in microwave tomography. We consider the scenario that consists of antennas placed at a distance away from the breast, both of which are immersed in some coupling medium. This is shown in Fig. 1.

Five algorithms have been implemented for this study. Their properties are reviewed in the following section.

A. DAS Algorithm

The signals transmitted from antennas undergo delay and attenuation as they reach the focal point and are reflected

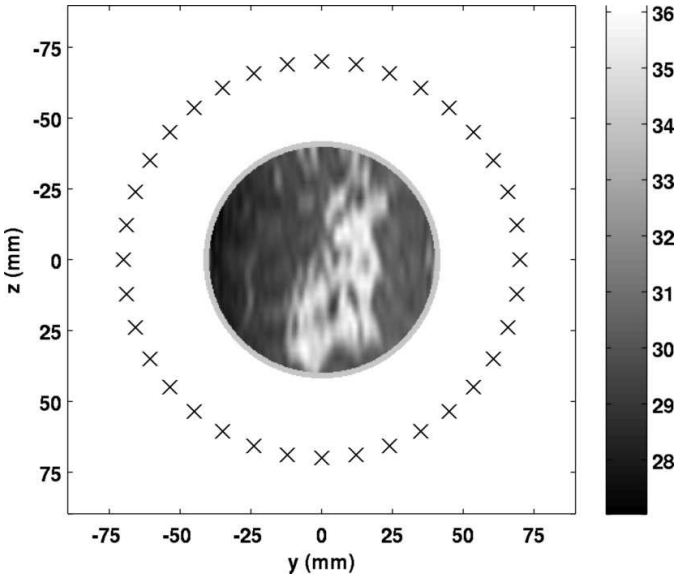

Fig. 1. Coronary slice of the permittivity extracted from one of the healthy breast phantoms. The locations of the current sources are marked by $\times$.

back to antennas. The DAS algorithm proposed in [3], [4] assumes the delay and attenuation of the propagation channels are modelled in the frequency domain as

$$\left(\frac{e^{-jk_{bg}d_{bg}}}{\sqrt{d_{bg}}} \frac{e^{-jk_{ts}d_{ts}}}{\sqrt{d_{ts}}} \right)^2 , \tag{1}$$

where d_{bg} and d_{ts} denote the propagation distances in the background medium and tissue, and k_{bg} and k_{ts} denote their wave numbers, respectively. The denominators denote the amplitude reduction due to the cylindrical spreading in 2-dimensional cases, and the numerators denote the delay and attenuation due to loss in the media. The power of two corresponds to the forward and backward propagation. Eq. (1) assumes operation in the far-field region. The effect of skin is not included due to its small electrical length. The DAS algorithm assumes the knowledge of k_{bg} and k_{ts} at the central frequency of the microwave pulse, and the knowledge of d_{bg} and d_{ts}. Thus, the effect due to the propagation channels, as predicted in (1), can be inverted. Then, the processed signals are time-gated to isolate the reflection at the focal point. They are summed, and the energy of the resulting signal denotes the pixel at the focal point.

B. DMAS algorithm

The DMAS algorithm [5] is a version of the DAS algorithm, which performs coupled cross-multiplication on the original mono-static signals. This artificially increases the number of input signals.

C. STB Algorithm

The STB algorithms formulated in the time domain [6] and in the frequency domain [7] assume the same channel model of (1). In addition, they invert the effect due to the propagation channels over all frequencies in the band of the tumor signals. Thus, k_{bg} and k_{ts} become complex vectors. The weights of the filters are the solutions to the wide-band equalization problem. The received signals are passed through the filters before being time-gated, summed, and having the energy calculated. The STB algorithm formulated in the frequency domain avoids the matrix inversion, which makes it very computationally efficient; thus, it is implemented in this study.

D. GLRT Algorithm

The GLRT algorithm [9] performs hypothesis testing of the presence of a tumor at each location, which is represented by computing the cross-correlation between the received signals and the signal templates. High correlation marks the presence of a tumor. The signal template used in this algorithm includes both the propagation and scattering of the microwave pulse, which is

$$\left(\frac{e^{-jk_{bg}d_{bg}}}{\sqrt{d_{bg}}} \right)^2 e^{-jk_{ts}(d_{ts}+a)} \sum_{n=-\infty}^{+\infty} (-j)^n a_n H_n^{(2)}(k_{ts}d_{ts}) \ ,$$

where the first term in the parenthesis describes the one-way propagation in the background, the second term denotes the forward propagation of a plane wave in the tissue, and the third summation term denotes the scattering by some tumor modelled as a dielectric cylinder [14]. Here $H_n^{(2)}$ denotes the n^{th}-order Hankel function of the second kind and the coefficient a_n is given by

$$a_n = \frac{\frac{\omega\epsilon_m}{k_m} J_n(k_{ts}a) J_n^{'}(k_m a) - \frac{\omega\epsilon_{ts}}{k_{ts}} J_n(k_m a) J_n^{'}(k_{ts}a)}{-\frac{\omega\epsilon_m}{k_m} H_n^{(2)}(k_{ts}a) J_n^{'}(k_m a) + \frac{\omega\epsilon_{ts}}{k_{ts}} J_n(k_{ts}a) H_n^{(2)'}(k_{ts}a)},$$

where ω is the angular frequency, a is the tumor radius and k_m is the complex tumor wave number. ϵ_t and ϵ_m are the relative permittivities of the healthy tissue and tumor, J_n denotes the n^{th}-order Bessel function, and $(\cdot)^{'}$ denotes the derivative with respect to the argument of the function.

E. RCB Algorithm

After the received signals are time aligned and compensated as in the DAS algorithm, the standard Capon beamformer produces a complex steering vector that minimizes the undesirable interference and noise contributions in the processed signals. The RCB algorithm [10] extends the standard Capon beamformer by permitting certain relaxation on the requirement of the steering vector up to some user-defined limit. This algorithm is developed to address the effects of not completely known propagation channels and other artifacts such as mismatches in antennae characteristics, mutual coupling, etc.

III. Experimental Methodology

A. Breast Models

In this work, the circular region of the breast tissue in a magnetic resonance image is extracted and enclosed by a 1.6-mm thick skin. The circular shape leads to identical skin-breast artifact seen at all antennas, which can be easily removed with, e.g., average-subtract algorithm. This allows us to focus on the results of the imaging algorithms.

TABLE I
TISSUE PROPERTIES FOR DATA SERIES

Series	Debye model parameters				Var (%)	$\min(\epsilon_{r,m}/\epsilon_{r,b})$	$\max(\epsilon_{r,m}/\epsilon_{r,b})$	$\min(\sigma_m/\sigma_b)$	$\max(\sigma_m/\sigma_b)$
	$\epsilon_{\infty,b}$	$\sigma_{s,b}$ (S/m)	$\Delta\epsilon$	τ (ps)					
1	3.1	0.05	1.6	13	7	10.6	11.1	24.8	25.1
2	13.0	0.4	24.4	13	30	1.4	1.6	1.7	1.8
3	13.0	0.4	24.4	13	70	1.3	1.7	1.7	1.8
4	13.8	0.7	35.6	13	30	1.1	1.2	1.2	1.2

The dielectric properties of tissue are described by the one-pole Debye model with four parameters: the relative permittivity for infinite value of frequency ϵ_∞, the difference between the infinite and static relative permittivity $\Delta\epsilon$, the static conductivity σ_s, the relaxation time constant τ [15]. As presented in Table I, for each series, the values of $\Delta\epsilon$ and τ of the pixels are assigned to some constants. The values of ϵ_∞, and σ_s are assigned according to the linear mapping from the pixel intensities to ϵ_∞ in the range of $\epsilon_{\infty,b}\,(1 \pm 0.01\mathrm{Var}/2)$ and to σ_s in the range of $\sigma_{s,b}\,(1 \pm 0.01\mathrm{Var}/2)$, where $\epsilon_{\infty,b}$ and $\sigma_{s,b}$ denote the mean values, and Var denotes the percentage of variation.

The selection of series properties can be explained as follows. Series 1 represents the case of the highest tumor-tissue contrast in dielectric properties and the lowest level of heterogeneity. This corresponds to adipose-dominant breast models and is the easiest case for the detection problem. Series 2 and 3 are based on the same contrast level, much lower than that for Series 1, and they differ in the level of heterogeneity. Series 3 represents a highly heterogeneous case. Series 4, having the contrast ratio close to 1, is considered to be the most difficult from the detection point of view and is referred to as "extremely dense". Average level of heterogeneity of 30% has been chosen for this series.

In Table I, column $\min(\epsilon_{r,m}/\epsilon_{r,b})$, $\max(\epsilon_{r,m}/\epsilon_{r,b})$, $\min(\sigma_m/\sigma_b)$, and $\max(\sigma_m/\sigma_b)$ represent the minimum and maximum ratios of the relative permittivity and conductivity between the tumor and the healthy tissue after the tissue assignment. The dielectric properties are evaluated at 6.85 GHz.

B. Finite-Difference Time-Domain Simulations

Fig. 1 shows an example of a breast model and the simulation scenario. The breast is placed in an oil-like lossless matching medium characterized by ($\epsilon' = 4.5, \sigma = 0$). A tumour with 3-mm radius, characterized by its Debye parameters ($\epsilon_\infty = 6.75$, $\sigma_s = 0.79$ S/m, $\Delta\epsilon = 48.35$, $\tau = 10.47$ ps), is placed inside the model. There are 36 equally-spaced current sources placed around the breast at a fixed distance (28 mm away from the skin). Each source sequentially emits a differentiated Gaussian pulse with a 3-dB bandwidth from 3.1 to 10.6 GHz. In this work, the mono-static scenario is considered, which gives 36 recorded signals for a breast model. The minimum wavelength determined by the largest permittivity at 10.6 GHz is 3.87 mm. We set the spatial increment to 0.4 mm and the relative Courant number to 0.999 to reduce the dispersion error. The time step is 2 ps. The maximum wavelength in the heterogeneous tissue at 3.1 GHz is 50.3 mm. We place 12 perfectly-matched layers at a half of this wavelength away from the sources to truncate the computation domain. Prior to the application of the imaging algorithms, we apply the average-subtract method to remove the skin-breast artifact. Then, the signals are down-sampled from 500 GHz to 64 GHz.

C. Data Sets

In order to provide sufficient statistics for the performance results assessment, we have generated ten different breast models containing tumor at different locations and applied them in the simulation procedure described above to obtain the signals received at each of the antennas. The same procedure has been applied to exactly the same tissue structures without tumour inside, which have been used for the assessment purposes.

For the GLRT algorithm, in addition to the ten realizations of tissue structure, thirty more realizations of healthy breast models have been produced to estimate the covariance matrices needed in the algorithm.

The same set of tissue structures with the assigned tumour locations have been used for each of the four series. The difference between the series is only in the tumor/tissue properties contrast and the level of heterogeneity. Besides the decrease in the number of breast phantoms needed for the experiments, fixing tissue structures between the series removes the factor of variability, which is beneficial for the performance comparison.

IV. RESULTS AND DISCUSSIONS

A. Performance metrics

The performance of the algorithms is evaluated based on the following metrics.

Correct Detection is a binary measure which shows if the location emphasized by the algorithm (image maximum) is attributed to the reflections from tumour rather than from the clutter. In order to check this, we subtract the image of the healthy breast model from the image of the breast model with a tumour inside. If the peak of the resulting image is within the 10-mm radius circle around the one detected by the algorithm in the tumorous image, we treat the detection as correct. Otherwise, we deem that the resulting image provides a misleading detection and is omitted in the subsequent analysis. Metrics presented further are only valid and computed in the cases of the correct detection.

TABLE II
NUMBER OF FALSE TUMOUR DETECTIONS

	Series 1	Series 2	Series 3	Series 4
DAS	0	0	0	10
DMAS	0	0	0	10
STB	0	1	1	9
GLRT	0	0	0	2
RCB	0	0	3	6

Signal-to-interference-and-noise ratio (SINR) - This metric is defined as

$$\mathrm{SINR} = 20\log\left(I_{\max,s}/I_{\max,n}\right), \tag{2}$$

where $I_{\max,s}$ and $I_{\max,n}$ correspond to the peak amplitudes of the tumorous and healthy images, respectively. The SINR is another important metric for the detection purpose. It shows the capability of the algorithms to discriminate tumorous breasts from healthy breasts.

Localization error (E_l) - Shows the distance between the true tumour location $\mathbf{c}$ and the one estimated by the algorithm $\hat{\mathbf{c}}$:

$$E_l = \|\mathbf{c} - \hat{\mathbf{c}}\|, \tag{3}$$

Peak-to-sidelobe ratio (PSLR) - This metric is defined as

$$\mathrm{PSLR} = 20\log\left(I_{\max,s}/I_{sl}\right), \tag{4}$$

where I_{sl} is the most significant sidelobe amplitude of a tumorous image. The contrast in the dielectric properties between tumorous and healthy tissue is correlated with the contrast of the breast images. The imaging algorithms cannot completely isolate the reflection due to the synthetic focal point. This leads to the presence of sidelobes in the images. PSLR is a metric to evaluate how well the imaging algorithms can preserve the dielectric contrast.

B. Discussion

The imaging algorithms descibed above have been applied to each of the data sets to obtain the described performance metrics. Fig. 2 - 4 summarize the results by organizing them into groups for each series. Only cases with correct detection have been taken into account to compute the average value and standard deviation of the metrics. When the algorithms cannot detect the tumour correctly in all ten cases, this fact is labelled as 'FAILED' on the figures.

Table II contains the number of incorrectly detected tumours for each series. Analyzing the table, it can be seen that most of the algorithms have troubles under the conditions of low contrast. The only reliable algorithm in such a scenario is the GLRT, which provides model of high complexity capable to describe the effects of scattering from the tumour. In conjunction with Fig. 2, one may notice that the simple algorithms such as DAS and DMAS are rather stable and successful under the high and medium tissue/tumor dielectric contrast levels. However, they fail under the extremely dense scenario. The STB algorithm, incorporating the effects of dispersion, exhibits marginal improvement over DAS and DMAS when the complexity of the model increases. The adaptive RCB algorithm demonstrates a gradual decrease in performance while the contrast decreases and heterogeneity grows. It is still capable to detect tumour in four cases out of ten in the extremely dense scenario. This is explained by its adaptive nature to the input data. By comparing Fig. 2 b) and c), it is seen that the increase in heterogeneity from 30% to 70% decreases SINR by 2 to 10 dB.

Fig. 3 gives the notion of tumour localization accuracy. It is observed that, for the easiest scenario, almost all of the algorithms localize the tumor up to the image resolution (1-mm grid). DAS/DMAS show equal results and outperform all other algorithms. The STB algorithm gives lower performance due to the point scatterer assumption, which favours locations in the deeper areas of the breast. Heterogeneity does not play important role for localization (compare Fig. 2, b) and c)).

The ability of the algorithms to isolate the tumour response by suppressing the clutter can be estimated from Fig. 4. First, we may emphasize the best performance of the RCB algorithm for the easiest scenario, which illustrates the adaptive capability of the algorithm. The good performance of the DMAS algorithm can be explained by the signals cross-multiplication between channels, which, in this case, acts as an effective clutter suppression mechanism. Similar to the SINR metric, the PSLR decreases by several decibels when the heterogeneity increases.

From the presented results, it is seen that the performance of the algorithms differs with respect to different metrics. This suggests that certain algorithms should be selected to address specific tasks. As the GLRT algorithm provides reliable detection in the sense of a good SINR in all series, it is considered for further extension and improvement.

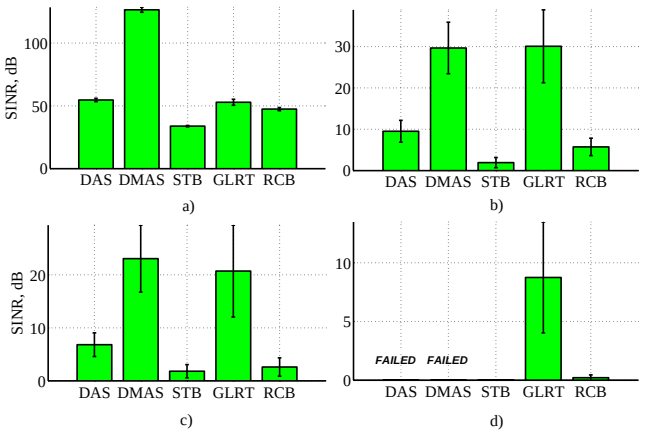

Fig. 2. Signal-to-interference-and-noise ratio for a) Series 1 b) Series 2 c) Series 3 and d) Series 4. Note that the scales in the four plots are not the same.

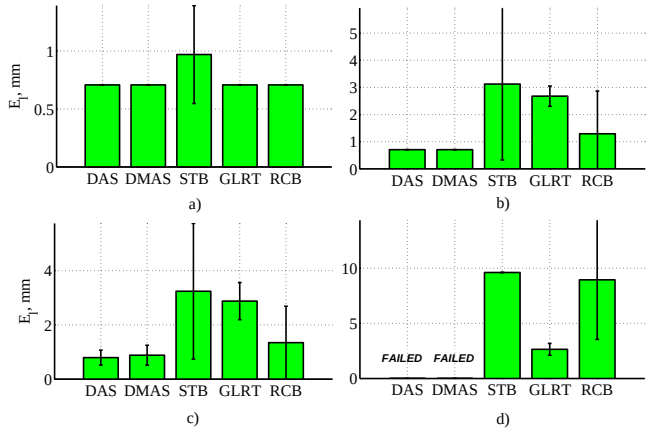

Fig. 3. Localization errors E_l for a) Series 1 b) Series 2 c) Series 3 and d) Series 4. Note that the scales in the four plots are not the same.

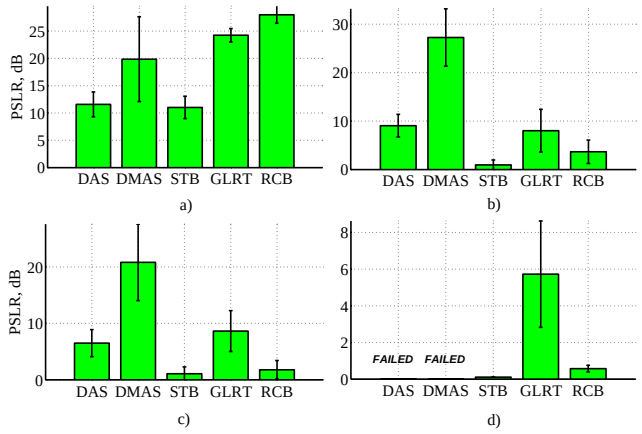

Fig. 4. Peak signal to sidelobe ratio a) Series 1 b) Series 2 c) Series 3 and d) Series 4. Note that the scales in the four plots are not the same.

V. Conclusions and Future Work

In this paper, we have studied the performance of five microwave breast imaging algorithms on the signals generated from the breast models with a reduced dielectric contrast and tissue heterogeneity. The GLRT algorithm is capable of detecting tumours, in the sense of a good SINR in comparison to DAS, DMAS, STB algorithms, and adaptive RCB algorithm. In this paper, we have assumed the average dielectric properties of the tissue and tumor as exactly known. In the future, we consider investigating how the parameters mismatch would affect the GLRT algorithm and extending it to handle multi-static signals for microwave breast imaging. The GLRT algorithm is also capable of handling signals from 3-D models. The challenge in these scenarios is to create multiple healthy breast models, which are needed to estimate the clutter covariance matrix.

Acknowledgment

The authors would like to acknowledge the support of the following funding agencies: Natural Sciences and Engineering Research Council of Canada and Le Fonds Québécois de la Recherche sur la Nature et les Technologies.

References

[1] M. Lazebnik, L. McCartney, D. Popovic, C. B. Watkins, M. J. Lindstrom, J. Harter, S. Sewall, A. Magliocco, J. H. Booske, M. Okoniewski, and S. C. Hagness, "A large-scale study of the ultrawideband microwave dielectric properties of normal breast tissue obtained from reduction surgeries," *Physics in Medicine and Biology*, vol. 52, no. 10, pp. 2637–2656, 2007.

[2] M. Lazebnik, D. Popovic, L. McCartney, C. B. Watkins, M. J. Lindstrom, J. Harter, S. Sewall, T. Ogilvie, A. Magliocco, T. M. Breslin, W. Temple, D. Mew, J. H. Booske, M. Okoniewski, and S. C. Hagness, "A large-scale study of the ultrawideband microwave dielectric properties of normal, benign and malignant breast tissues obtained from cancer surgeries," *Physics in Medicine and Biology*, vol. 52, no. 20, pp. 6093–6115, 2007.

[3] X. Li and S. C. Hagness, "A confocal microwave imaging algorithm for breast cancer detection," *IEEE Microwave Wireless Compon. Lett.*, vol. 11, no. 3, pp. 130–132, 2001.

[4] E. C. Fear, X. Li, S. Hagness, and M. A. Stuchly, "Confocal microwave imaging for breast cancer detection: localization of tumours in three dimensions," *IEEE Trans. Biomed. Eng.*, vol. 49, no. 8, pp. 812–822, 2002.

[5] H. B. Lim, N. T. T. Nhung, E.-P. Li, and N. D. Thang, "Confocal microwave imaging for breast cancer detection: delay-multiply-and-sum image reconstruction algorithm," *IEEE Trans. Biomed. Eng.*, vol. 55, no. 6, pp. 1697–1704, 2008.

[6] E. J. Bond, X. Li, S. C. Hagness, and B. D. van Veen, "Microwave imaging via space-time beamforming for early detection of breast cancer," *IEEE Trans. Antennas Propagat.*, vol. 51, pp. 1690–1705, 2003.

[7] S. K. Davis, E. J. Bond, X. Li, S. C. Hagness, and B. D. van Veen, "Microwave imaging via space-time beamforming for early detection of breast cancer: beamformer design in the frequency domain," *Journal of Electromagnetic Waves and Applications*, vol. 17, no. 3, pp. 357–381, 2003.

[8] P. Kosmas and C. Rappaport, "FDTD-based time reversal for microwave breast cancer detection-localization in three dimensions," *IEEE Trans. Microwave Theory Tech.*, vol. 54, no. 4, pp. 1921–1927, 2006.

[9] S. K. Davis, H. Tandradinata, S. C. Hagness, and B. D. van Veen, "Ultrawideband microwave breast cancer detection: a detection-theoretic approach using the generalized likelihood ratio test," *IEEE Trans. Biomed. Eng.*, vol. 52, no. 7, pp. 1237–1250, 2005.

[10] B. Guo, Y. Wang, J. Li, P. Stoica, and R. Wu, "Microwave imaging via adaptive beamforming methods for breast cancer detection," *Journal of Electromagnetic Waves and Applications*, vol. 20, pp. 53–63, 2006.

[11] Y. Xie, B. Guo, J. Li, G. Ku, and L. V. Wang, "Adaptive and robust methods of reconstruction for thermoacoustic tomography," *IEEE Trans. Biomed. Eng.*, vol. 55, pp. 2741–2842, 2008.

[12] M. O'Halloran, M. Glavin, and E. Jones, "Performance and robustness of a multistatic mist beamforming algorithm for breast cancer detection," *Progress in Electromagnetics Research*, vol. 105, pp. 403–424, 2010.

[13] D. Byrne, M. O'Halloran, E. Jones, and M. Glavin, "Transmitter-grouping robust capon beamforming for breast cancer detection," *Progress in Electromagnetics Research*, vol. 108, pp. 401–416, 2010.

[14] R. F. Harrington, *Time-Harmonic Electromagnetic Fields*. Piscataway, NJ: IEEE Press, 2001.

[15] A. Sihvola, *Electromagnetic Mixing Formulas and Applications*. London, UK: The Institution of Electrical Engineers, 1999.